

# Effect of Hot Streak Migration on Unsteady Blade Row Interaction in an Axial Turbine

P. Jenny<sup>1</sup>

e-mail: jenny@lec.mavt.ethz.ch

C. Lenherr

R. S. Abhari

Laboratory for Energy Conversion,  
Department of Mechanical and Process  
Engineering,  
ETH Zurich,  
Zurich, Switzerland

A. Kalfas

LFMT, Department of Mechanical Engineering,  
Aristotle University of Thessaloniki,  
GR-54124 Thessaloniki, Greece

*This paper presents an experimental study of the effect of unsteady blade row interaction on the migration of hot streaks in an axial turbine. The hot streaks can cause localized hot spots on the blade surfaces in a high-pressure turbine, leading to high heat loads and potentially catastrophic failure of the blades. An improved understanding of the effect of unsteady blade row interaction on an inlet temperature distortion is of crucial importance. The impact of hot streaks on the aerodynamic performance of a turbine stage is also not well understood. In the current experiment, the influence of hot streaks on a highly loaded 1.5-stage unshrouded model axial turbine is studied. A hot streak generator has been developed specifically for this project to introduce hot streaks that match the dimensional parameters of real engines. The temperature profile, spanwise position, circumferential position, and cross-section shape of the hot streak can be independently varied. The recently developed ETH Zurich two-sensor high temperature (260°C) fast response aerodynamic probe (FRAP) technique and the fast response entropy probe (FENT) systems are used in this experimental campaign. Time resolved measurements of the unsteady pressure, temperature, and entropy are made at the NGV inlet and between the rotor and stator blade rows. From the nozzle guide vane inlet to outlet the measurements show a reduction in the maximum relative entropy difference between the free stream and the hot spot of 30% for the highest temperature gases in the core of the hot streak, indicating a region of heat loss. Time resolved flow field measurements at the rotor exit based on both measurement methods showed the hot gases traveling towards the hub and tip casing on the blade pressure side and interacting with secondary flows such as the hub passage vortex. [DOI: 10.1115/1.4004447]*

## Introduction

In order to improve the efficiency and performance of modern gas turbines, designers constantly strive to increase the turbine entry temperature. Experimental data taken from gas turbine combustor exit flows appear to have strong radial and circumferential temperature gradients, often referred to as hot streaks or hot spots. These pronounced temperature non uniformities in the combustor exit flow field are caused by circumferentially discrete fuel and dilution air injection within the combustor. The hot streaks interact with the different turbine parts and can locally cause increased blade heat transfer leading to reduced blade life and significant risks. As a consequence, turbine components are generally designed for higher temperatures than the mean turbine entry temperature. As the induced migration physics cannot be quantitatively predicted with satisfactory accuracy for the hot gases, turbine designers need to budget for the worst case temperature distortions. An improved understanding of hot streak thermally driven transport mechanisms and unsteady blade row interactions is required to set up an effective blade cooling strategy in order to minimize the use of performance costing cooling flow in the turbine.

One of the earliest studies of inlet flow distortion effects on a stationary blade row was undertaken by Munk and Prim in 1947 [1]. It has been shown for inviscid steady flow that the stream line pattern in a vane passage is theoretically not influenced by the presence of a variation in total temperature as long as the stagnation pressure distribution remains constant, or more precisely, as long as the absolute momentum distribution remains unaltered. Hermanson and Thole [2] showed that the driving parameter for

secondary flow generation in a turbine vane is the stagnation pressure distribution. Experimental studies on the transport mechanisms of combustor exit stagnation pressure and temperature profiles conducted in a high pressure turbine vane by Barringer et al. [3] show a significant effect of the near end wall stagnation pressure profile on the redistribution of the stagnation enthalpy on its way through the vane. The induced changes in heat transfer on high pressure vanes and end walls have been experimentally and numerically analyzed by Povey et al. [4] and Barringer et al. [5]. The combined effect of high turbulence and film cooling on the mixing and dispersion of a hot spot in a nozzle guide vane was experimentally studied by Jenkins et al. [6]. It was shown that turbulence effects and film cooling considerably reduce the hot spot peak temperatures.

The thermally driven effects of an inlet temperature distortion on the rotor flow field are more complex. In the absolute frame the hot air travels at the same absolute momentum and flow angle as the free stream. In a rotor relative view the hot gases have a higher relative momentum and thus higher relative stagnation pressure. Whereas variations in stagnation pressure generate secondary flows in a stationary blade row, the gradients in relative stagnation pressure induced by a hot spot are a source of additional secondary flows. The preferential migration of hot gases towards the pressure side and cold gases towards the suction side, as well as the migration of the hot gases towards the end walls once they arrive on the pressure side were first experimentally observed by Butler et al. [7] and experimentally verified by Roback and Dring [8]. Three dimensional unsteady computational investigations by Dorney et al. [9] and Rai et al. [10] have reported similar findings. The tendency for separation of hot and cold gases was first mentioned by Kerrebrock et al. [11] in their work on the effect of the high temperature compressor rotor wakes on downstream stator blades. Assuming a steady and incompressible flow and neglecting circumferential gradients, Butler et al. [7] show that in a rotating blade row the generation of streamwise

<sup>1</sup>Corresponding author.

Contributed by the International Gas Turbine Institute (IGTI) of ASME for publication in the JOURNAL OF TURBOMACHINERY. Manuscript received March 16, 2011; final manuscript received June 3, 2011; published online May 29, 2012. Editor: David Wisler.

vorticity is a function of relative radial stagnation pressure and density gradients. The time resolved transport mechanisms in the rotor flow field have only rarely been addressed to date in the open literature and are mainly based on CFD results. The unsteady migration of injected coolant mass flow in a turbine rotor flow field has been investigated and analyzed by Ong et al. [12] and An et al. [13].

The aim of this work is to analyze the unsteady transport mechanisms generated by an inlet temperature distortion, based on the results of an experimental measurement campaign that was carried out in a model real engine like test turbine environment. The effect of the NGV and the rotor on the hot streak and the unsteady interaction between rotor and stator blade rows are analyzed in detail with particular attention being paid to the unsteady thermally driven transport mechanisms. In addition to these experimental results, a numerical study carried out by Basol et al. [14] analyzes the effect of the hot streak's position at the NGV inlet on the stage heat load and in particular on the rotor blade tip.

## Experimental Method

The experimental investigation was performed in the research turbine "LISA" in the Turbomachinery Laboratory at ETH Zurich. The existing two-stage, shrouded turbine configuration was redesigned as a 1.5-stage unshrouded turbine which is representative of a high work, cooled turbine. Further details of the new design are presented by Behr et al. [15]. Its salient features are described below. For this experimental study on hot streaks, an inlet temperature distortion generator was added to the existing 1.5-stage unshrouded turbine upstream of NGV1.

**Experimental Turbine Facility.** The air loop of the facility is quasi-closed and includes a radial compressor, a two-stage water to air heat exchanger, and a calibrated venturi nozzle for mass flow measurements. Upstream of the turbine section is a 3 m flow conditioning stretch to ensure a homogenous flow field. Additionally the flow undergoes an acceleration ahead of the turbine section in order to reduce the significance of the remaining flow uniformities from upstream. At the exit of the turbine section the air loop opens to the atmosphere. A dc generator absorbs the turbine power and controls the rotational speed with an indicated accuracy of  $\pm 0.02\%$  ( $\pm 0.5$  rpm). A heat exchanger controls the inlet total temperature  $T_{i,in}$  with an accuracy of  $\pm 0.3\%$ . A torque-meter measures the torque on the rotor shaft. With the compressor ratio limited to  $\Pi_{c,max} = 1.5$  it is necessary to add a tandem deswirl vane arrangement to recover the static pressure at the exit of the second stator back to the ambient level, in order to reach the intended turbine pressure ratio of  $\Pi_{1.5} = 1.65$ . The turbine is unshrouded with a nominal tip gap of 1% of the span. The variation of the tip gap between two builds is less than 1% of the tip gap, which ensures good repeatability. At the exit of the first nozzle guide vane row the flow is compressible with an exit Mach number of 0.53.

**Inlet Temperature Distortion Generator.** The temperature distortion generator is designed to introduce one single hot spot upstream of the first nozzle guide vane row, allowing mixing ahead of the NGV1 inlet plane. The hot streak was generated by passing a bypass flow through an external flow heater and blower before reintroducing the heated flow through circular injector pipes with a diameter of 30% span. The injector pipes were mounted on a vane shaped support strut to minimize the main flow disturbance. The hot streak outlet plane is approximately 3.5 NGV1 axial chords upstream of the first nozzle inlet plane. Figure 1 shows a cut through the turbine with the hot streak generator. The strut is represented in blue and the red part represents the injection pipes for the hot air. The design was such that it allowed variation of the NGV1 clocking angle and the radial position of the hot streak (from about 20% to about 65% span) as well as the

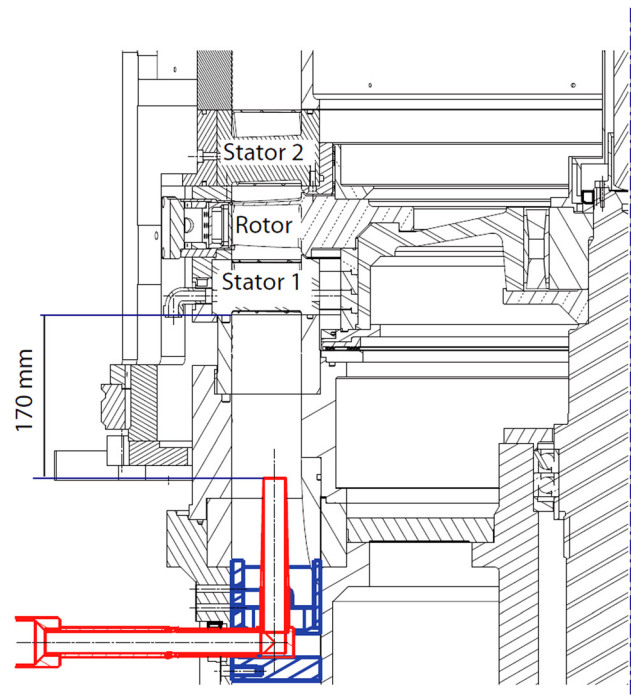


**Fig. 1** Cut through the 1.5-stage unshrouded turbine with hot streak generator upstream of NGV1

cross-sectional shape of the hot streak outlet. In the current study the hot streak generator was located at 50% span and circumferentially positioned at midpitch so that the hot streak does not impinge on the blades. The bypassed air can be heated to a maximum peak temperature over free stream ratio of 1.35 allowing for different temperature profiles.

**Measurement Technology.** The unsteady flow field was measured using a recently developed high temperature fast response aerodynamic probe (HT-FRAP) and the fast entropy probe (FENT). The characteristics of the standard FRAP probe (Kupferschmid et al. [16]) allow its use in flow fields up to  $120^\circ\text{C}$ . The recently developed high temperature FRAP probe was designed in the LEC at ETH Zurich (Lenherr et al. [17]) and allows measurements to be taken in higher temperature flows up to  $260^\circ\text{C}$ . As for the standard FRAP probe the primary elements are two piezoresistive pressure transducers that are used to measure the unsteady pressure and unsteady velocity field, as well as the steady temperature. Additional temperature and strain gauge sensors are embedded in the shaft of the high temperature FRAP probe to allow a much higher degree of robustness in the use of this probe. The probe is capable of capturing unsteady flow features up to frequencies of 25 kHz based on measurements including total and static pressures, flow yaw and pitch angles, and Mach number. The frequency bandwidth of the temperature is limited to a frequency of 10 Hz. However the influence of the measured temperature on the velocity is very modest. The high temperature FRAP probe has a 2.5 mm tip diameter and is equipped with two sensors. The probe is operated in a virtual-four-sensor mode to measure three-dimensional, time resolved flow properties. The data is acquired at a sampling rate of 200 kHz over a period of 2 s. The post-processing is done for three consecutive rotor pitches. The sampling rate resolves 82 points in the relative frame of reference. Table 1 gives the relative measurement uncertainties of the FRAP probe as a percentage of the calibration range of  $\pm 24$  deg for the yaw angle,  $\pm 20$  deg for the pitch angle, and as a percentage of the dynamic head for total and static pressure.

The time resolved temperature measurements were carried out with the fast response entropy probe (FENT probe) designed and

**Table 1 Relative uncertainty of the high temperature FRAP probe**

Yaw angle	Pitch angle	$P_t$	$P_s$
1.1%	2.0%	1.1%	1.3%

developed at the LEC at ETH Zurich by Mansour et al. [18], [19]. The probe has a diameter of 1.8 mm and is comprised of two parts. First, a miniature silicon piezoresistive chip is glued beneath a pressure tap to measure the unsteady static and total pressures. Second, a pair of thin film gauges with a thickness of about 200 nm are operated as resistance thermometers at two different film temperatures, and used to measure the unsteady total temperature. Knowing unsteady total temperature  $T_t$  and total pressure  $P_t$ , the unsteady relative entropy can be calculated using Eq. (1):

$$\Delta s = C_p \ln \frac{T_t}{T_{t,ref}} - R \ln \frac{P_t}{P_{t,ref}} \quad (1)$$

The serpentine shaped thin films cover a rectangular area of 1.77 mm × 0.85 mm. The radial distance covered by the serpentine shaped thin films, representing 2.52% of the passage height in the measurement plane, is the minimum spatial resolution on the measurement grid. The measurements taken with the FENT probe have a radial spacing of 1.125 mm in the regions of radial clustering and of 2.25 mm elsewhere. In the data processing, coincident phase-locked measurements of  $P_t$  and  $T_t$  are used to determine the unsteady relative entropy. The measurement bandwidth is 48 kHz, and data are acquired at a sampling frequency of 200 kHz over a period of 2 s, as for the high temperature FRAP probe. The absolute uncertainties in the measurements and derived quantities are summarized in Table 2. As unsteady temperature and pressure are measured at different locations in the same probe, the data is shifted in the radial direction by the distance between the two measurement holes during the post-processing in order to have both signals from exactly the same location before calculating the entropy.

**Measurement Planes.** The data was measured at three different traverse planes in the turbine test facility. Figure 2 shows the geometry and the relative positions of stators one and two, as well as the relative position of the three traverse planes, S1inlet, S1ex, and R1ex. At traverse planes S1ex and R1ex the spatial resolution of the measurement grid consisted of 45 radial and 41 equally spaced points in the circumferential direction covering one stator pitch. For traverse plane S1in only 80% of a pitch is covered, representing a spatial resolution of 45 radial and 33 circumferential points. The measurement grid has a radial clustering near the end walls and at the hot streak location. The data is acquired at a sampling rate of 200 kHz over a time period of 2 s. Within these 2 s three blade passing events are phase-lock averaged 82 times.

**Operating Conditions.** During the measurements the turbine 1.5-stage total-to-static pressure ratio is kept constant at  $\Pi_{1.5} = 1.65$ , conforming with former test campaigns using the same turbine (Table 3). The entry and hot streak temperatures are kept uniform to permit an accurate comparison between measurements made on different days. To account for the change in ambient pressure on different measurement days the pressures are

**Table 2 Uncertainty bandwidth of the FENT probe**

$P_t$	$T_t$	$\Delta s$
0.1%	2.5%	2.51%

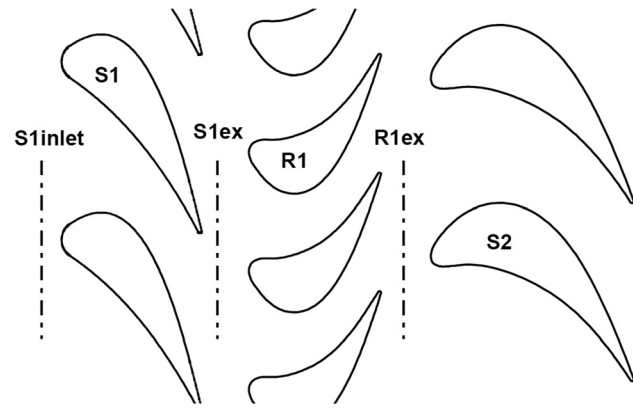


**Fig. 2 Illustration of geometrical relations and measurement planes**

nondimensionalized by the respective inlet total pressure. The hot streak mass flow was adapted such that its stagnation pressure and Mach number were at the same level as the free stream in order to represent real engine conditions.

## Results and Discussion

In the following section the time-resolved flow field data are presented paying particular attention to the thermally driven transport mechanisms. The analysis will start with the effect of the nozzle guide vane on the hot streak and then discuss the unsteady flow features created by the inlet temperature distortion. Data measured at two different hot streak temperatures are discussed. As the FENT probe is limited to flow temperatures not exceeding 110 °C, a first measurement set was undertaken with the FENT probe where the peak to free stream stagnation temperature ratio was  $T_{peak}/T_{free\ stream} = 1.21$ . The recently developed high temperature FRAP probe allowed a second measurement set with a higher hot streak outlet temperature  $T_{peak}/T_{free\ stream} = 1.36$ .

**NGV Inlet Flow Field.** Figure 3 represents the time averaged normalized total temperature measured by the FENT probe at the nozzle guide vane inlet plane. The hot spot has a circular shape and is located at about 50% span. In the core of the hot spot the peak to free stream stagnation temperature ratio is at the same level as at the outlet of the generator pipe  $T_{peak}/T_{free\ stream} = 1.21$ . In the periphery the hot air started mixing out with the free stream before arriving at the NGV1 inlet measurement plane. A more detailed picture is given by the radial distribution of the time and circumferentially mass averaged normalized stagnation temperature in Fig. 4. This graph also contains the data acquired with the high-temperature FRAP probe at the same axial position but at higher hot spot temperature ( $T_{peak}/T_{free\ stream} = 1.36$ ). Both measurement techniques show the center of the hot streak to be located at about 50% span and its width at the base to be about 50% span due to mixing before arriving at the NGV1 inlet.

**Table 3 Operating conditions and geometrical characteristics**

$\Pi_{1.5}$	$1.65 \pm 0.4\%$ (–)
$T_{t,in}$	$314 \pm 0.2$ (K)
$\dot{m}\sqrt{T_{t,in}}$	$151.6 \pm 0.2\%$ ( $kg\ K^{1/2}/s\ bar$ )
$\frac{P_{t,in}}{N}$	$2.54 \pm 0.05$ (rps/K <sup>1/2</sup> )
Mach no. (S1inlet/S1ex/R1ex)	0.14/0.52/0.24 (–)
Re (S1/R1/S2)	$7.1/3.8/5.1 \times 10^5$ (–)
Blade count (S1/R1/S2)	36/54/36 (–)
Aspect ratio (S1/R1/S2)	0.87/1.17/0.82 (–)

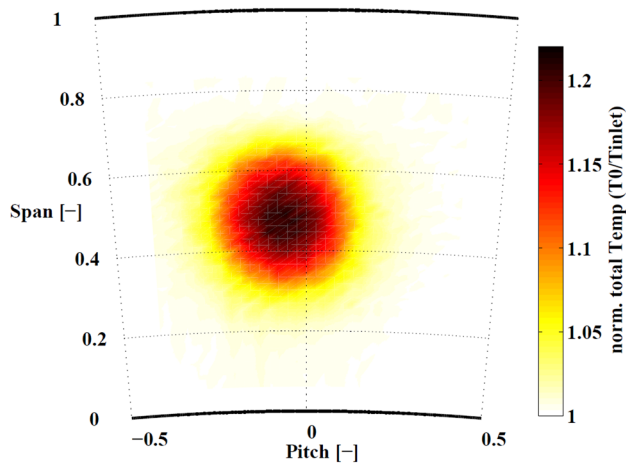


**Fig. 3** Time averaged normalized total temperature at the NGV1 inlet with hot streak ( $T_{peak}/T_{free\ stream} = 1.21$ )

**NGV Exit Flow Field.** Figure 5 compares the circumferentially mass and time averaged normalized stagnation temperature profiles at the nozzle inlet and outlet showing a reduction in the maximum circumferentially mass weighted normalized stagnation temperature  $\bar{T}_{mottmax}^{circ}$  of about 20% for both measurement cases. Additionally, the temperature profile has grown wider in the radial direction on its way through the nozzle guide vane, especially on the hub side of the hot spot. This indicates that heat conduction and mixing are taking place. The peak of the circumferentially mass averaged temperature profiles has moved about 4% towards the hub end wall. The radial migration towards the hub end wall is mostly due to lower static pressure levels at the hub end wall at S1ex. A more precise picture can be drawn from the time resolved unsteady temperature field at the nozzle exit. Equally spaced time snapshots of the normalized unsteady temperature field covering one rotor blade passing period  $T$  have been plotted in Fig. 6. During one rotor blade passing period the highest temperature gases in the center of the hot spot at S1ex travel about 20% of a pitch in the circumferential direction. This unsteady movement is dominated by the downstream rotor potential pressure field, as according to Munk and Prim [1] the inlet temperature distortion does not create any secondary flows in a stationary blade row acting on the shape of the hot streak. The instantaneous position of the rotor blades creates a quasi-steady effect. When a rotor blade is approaching the hot spot it is first entrained by the rotor potential

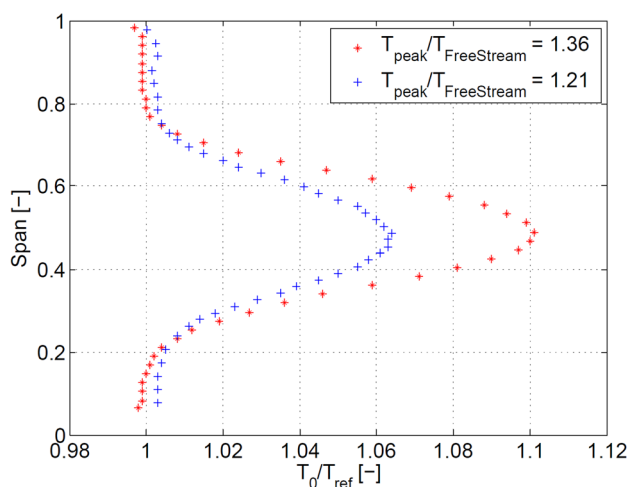


**Fig. 4** Circumferentially mass and time averaged normalized total temperature at the NGV1 inlet plane for the two measurement cases

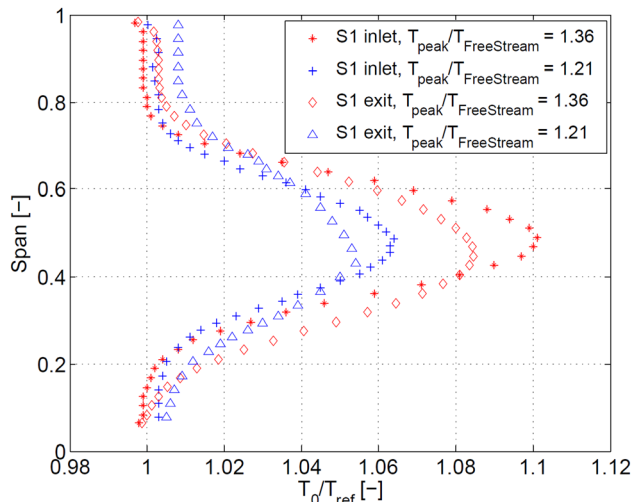


**Fig. 5** Comparison of circumferentially mass and time averaged normalized total temperature at the NGV1 inlet and exit planes for the two different test cases

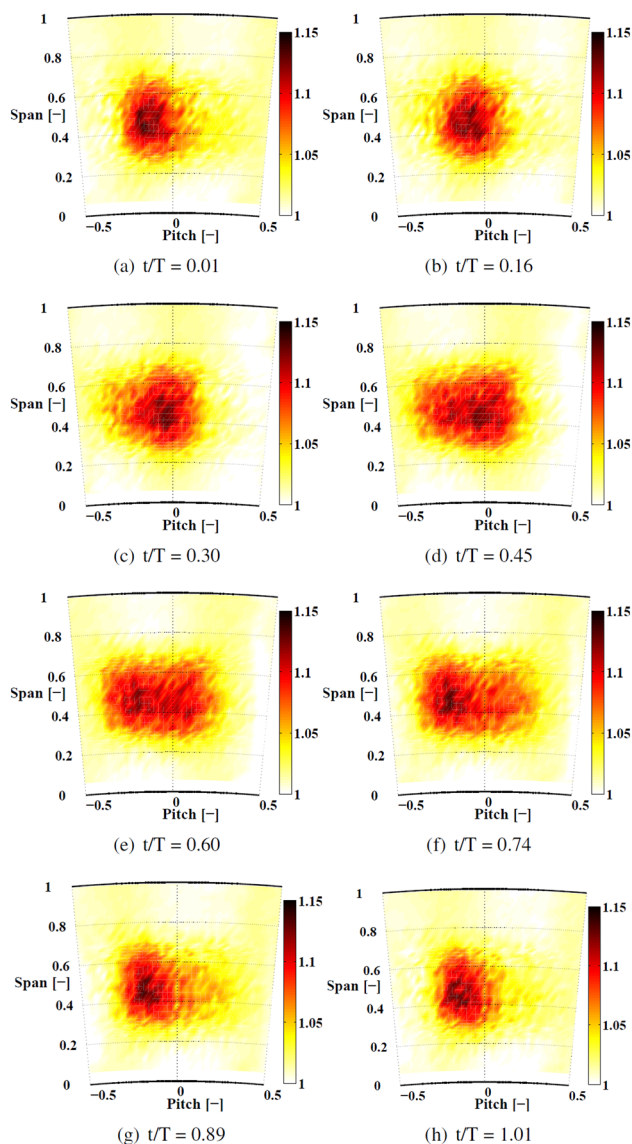


**Fig. 6** Normalized stagnation temperature for different time steps at traverse plane S1ex ( $T_{peak}/T_{free\ stream} = 1.21$ )

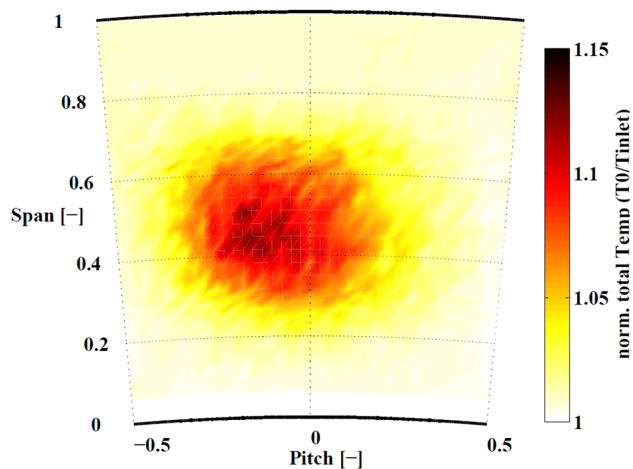


Fig. 7 Time averaged normalized stagnation temperature at S1ex plane ( $T_{\text{peak}}/T_{\text{free stream}} = 1.21$ )

field, at a certain point the hot air flips around the rotor leading edge and travels to the pressure side and is then entrained by the rotor potential field. This variation of the flow yaw angle causes an unsteady wobbling movement of the hot streak in the circumferential direction at the rotor blade passing frequency, as has been reported by Shang and Epstein [20]. In a time averaged view of the stagnation temperature (Fig. 7) this wobbling effect results in an oval shape in the circumferential direction of the hot streak at the nozzle exit amplified by the relatively high absolute average flow angle of 75 deg at this location. The highest temperature gases are not centered in the hot spot anymore in the time averaged total temperature field at S1ex, showing that the hot streak is more diffused towards the suction side (right hand side of Fig. 7) due to the effect of the nozzle guide vane. An et al. [21] have reported similar findings on the effect of a nozzle guide vane on hot streaks.

At the nozzle guide vane inlet plane the maximum measured unsteady difference in stagnation temperature between the hot spot and the free stream was  $\Delta T_{\text{max}} = 65$  K for the first test case based on the FENT measurements. At S1ex  $\Delta T_{\text{max}}$  has dropped by about 30% compared to the inlet plane. This indicates a strong mixing activity including an unsteady transport mechanism in the nozzle guide vane, which is a function of the inlet turbulence level and length scale. The turbulence level at the nozzle inlet plane was measured using the high temperature FRAP probe. The measured time averaged turbulence intensity based on the nondeterministic parts of the three Cartesian components of the absolute flow velocity vector is about 6% to 7% inside the hot streak and in the free stream. This level of turbulence enhances the mixing taking place in the nozzle guide vane. When analyzing the significant

drop in  $\Delta T_{\text{max}}$ , one has to keep in mind that the FENT probe provides deterministic unsteady total temperature data  $\bar{T}_t + \tilde{T}_t(t)$  using the triple decomposition of the time-resolved temperature signal according to Eq. (5). The random fluctuations  $T'_t$  involve higher temperatures (some of the time) than the deterministic mean recorded. As a consequence, the reduction of  $\Delta T_{\text{max}}$  is due to both mixing and also ensemble averaging. The importance of the averaging effect compared to the mixing has not been assessed. In order to exclude heat loss in the nozzle guide vane or measurement error, a mass weighted area integral at the inlet to and exit from the NGV of the stagnation enthalpy flux was performed. For each cell defined by the measurement grid the instantaneous total enthalpy flux was computed and then time averaged over one measurement period. As shown in Eq. (2) the time averaged total enthalpy flux of all cells was then added to give the total enthalpy flux through the measurement area:

$$\dot{H}_t = \sum_{\text{cells}} C_p(t) T_t(t) \rho(t) V_x(t) A_{\text{cell}} \quad (2)$$

The difference in measured total enthalpy flux between the nozzle inlet and outlet was about 0.7% showing that steady operating conditions were achieved for this test rig for the measurements and that very little enthalpy was lost in the nozzle guide vane through the end walls.

Figure 8 shows the time averaged relative entropy at the nozzle inlet and outlet based on the unsteady computation of entropy using Eq. (1) with  $T_{\text{ref}} = T_{\text{inlet}}$  and  $P_{\text{ref}} = P_{\text{inlet}}$ . The relative entropy in the hot spot is higher due to the temperature term in the entropy equation assuming uniform stagnation pressure at the inlet and giving the plot the same shape as for the NGV inlet total temperature (Fig. 3). The maximum difference of relative entropy between hot spot and free stream  $\Delta s_{\text{max}}$  reduces by 30% on its way through the nozzle guide vane (Fig. 8). The effect of the downstream rotor unsteady potential pressure field is also visible in the time averaged entropy plot, in the same way as for the time averaged total temperature at the nozzle exit, as the entropy calculation is driven by the stagnation temperature. The high entropy zones of the hot spot are stretched in the circumferential direction. According to the second law of thermodynamics:

$$q \leq T \Delta s \quad (3)$$

there is a relationship between the total heat transferred to the particle between the nozzle inlet and exit  $q$ , its temperature  $T$ , and specific entropy change  $\Delta s$ . Following the analysis presented by Rose [22], the term on the right hand side of inequality (3) becomes negative in the case of the highest temperature streak gas losing entropy. Therefore the only possible explanation for the reduction of entropy is particle heat loss. Looking at the entropy transport equation from the literature

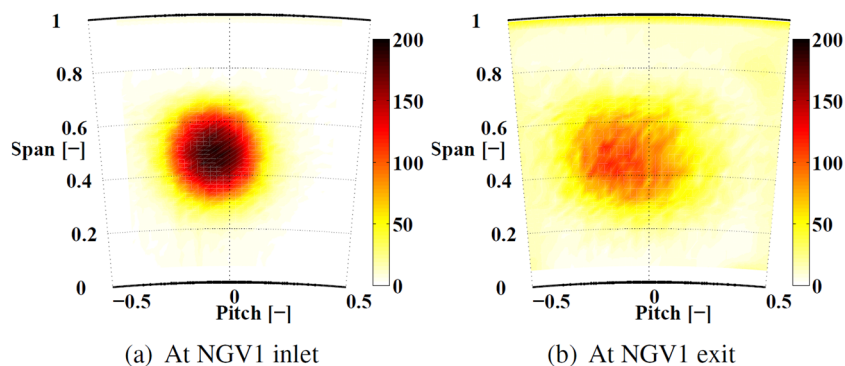
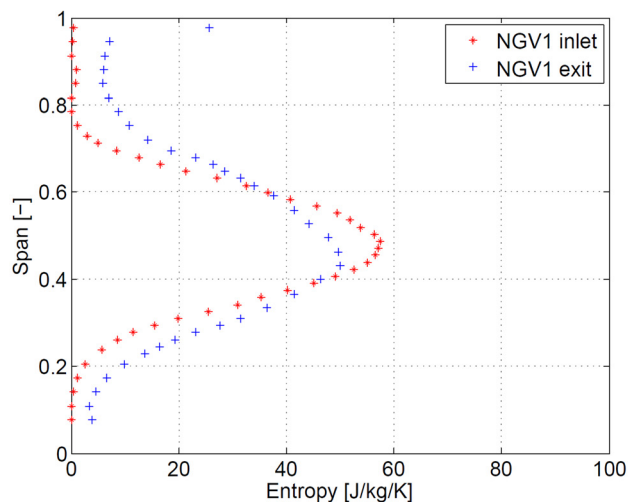
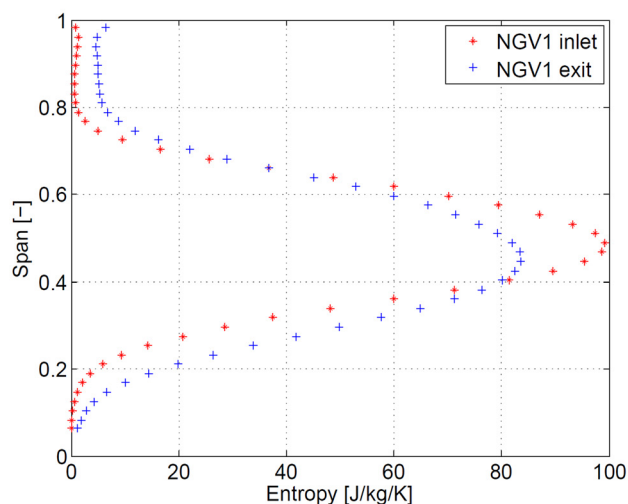


Fig. 8 Time averaged total entropy at NGV1 inlet and outlet ( $T_{\text{peak}}/T_{\text{free stream}} = 1.21$ )

(a) Case 1,  $T_{peak}/T_{freestream} = 1.21$  (FENT data)(b) Case 2,  $T_{peak}/T_{freestream} = 1.36$  (FRAP data)

**Fig. 9** Circumferentially mass and time averaged total entropy at NGV1 inlet and exit measurement plane for the two measurement cases

$$\rho \frac{Ds}{Dt} = -\nabla \left( \frac{\bar{q}}{T} \right) + \frac{\Phi_{Dis}}{T} + \frac{\Phi_{Cond}}{T^2} \quad (4)$$

only the first term representing the heat flux due to internal heat transfer can be negative. For the gases of the hot streak losing relative entropy on their way through the nozzle guide vane, the  $\Delta s$  can only be negative due to the diffusion of heat away from the hot streak. The negative term in the entropy transport equation must also balance out the entropy generation related to the dissipation of kinetic energy and the conduction of heat [second and third terms of Eq. (4)]. The velocity of the hot streak is higher than the velocity of the free stream because it is hotter. Therefore there is viscous dissipation taking place, in particular at the interface with the free stream, generating entropy.

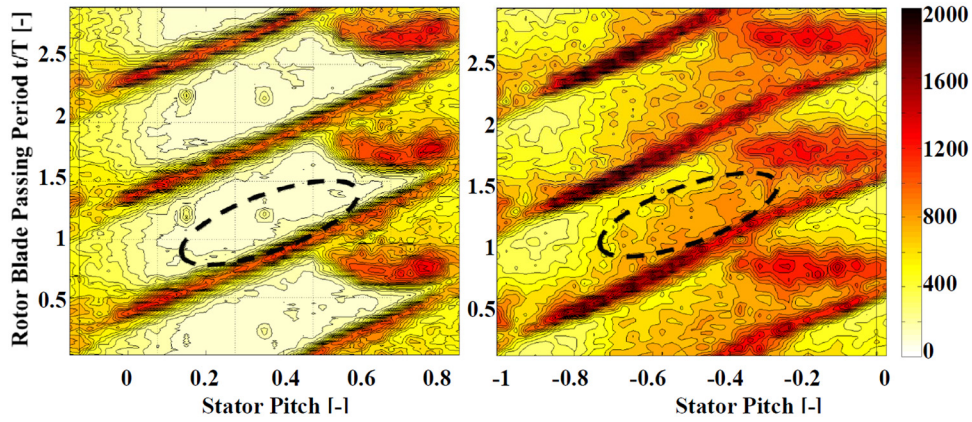
Figure 9 compares the time and mass averaged entropy at the NGV inlet and exit for the two measurement cases with different hot spot temperatures. Looking first at the time averaged unsteady FENT measurements, the mass weighted maximum entropy falls for the core of the hot streak from the NGV1 inlet to the outlet by about 12%, clearly indicating heat loss. With increasing radius from the center of the hot streak the viscous dissipation and ther-

mal conduction terms first balance out the heat loss and then become dominant. As a consequence the entropy difference becomes positive and joins the free stream level. The free stream entropy level has increased between the NGV1 inlet and outlet. This is a consequence of the circumferential mass averaging procedure over one stator pitch including the nozzle guide vane secondary flow wake losses. Shifting the curve for S1ex in order to match the free stream entropy levels at the nozzle inlet and outlet facilitates removal of the secondary flow wake losses. In this case, the central heat loss region becomes more pronounced and the dissipation and conduction dominated regions are pushed further out. The effect of the casing boundary layer on the entropy generation between the nozzle inlet and outlet is the reason for the increased relative entropy level of the closest point to the casing in Fig. 9. The second plot in Fig. 9 gives the relative entropy generation calculated based on the FRAP probe, providing unsteady pressure and time averaged temperature measurements. The same conclusions can be drawn as from the FENT data, allowing for the fact that the curve has a smoother shape due to the time averaged temperature acquisition. The overall mass weighted relative entropy integral increases for both measurement cases by about 8% from the nozzle guide vane inlet to outlet.

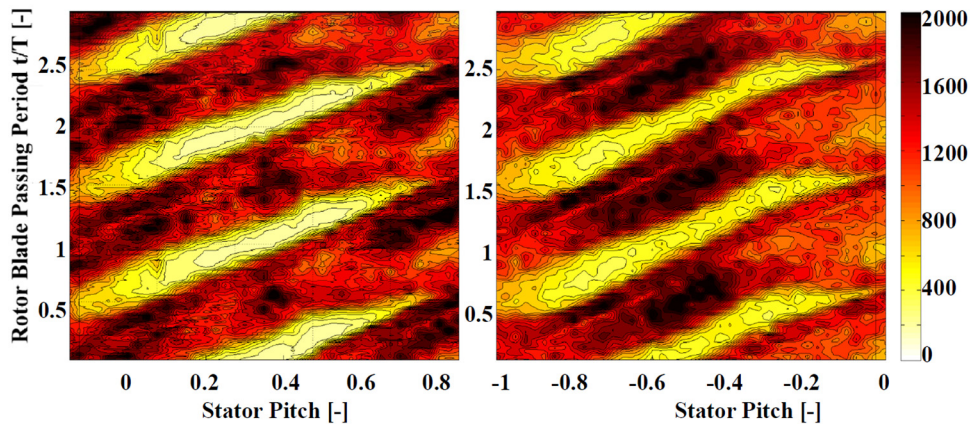
**Rotor Exit Flow Field.** The unsteady blade row interactions on the migration of the hot streak are examined next. In order to track the hot streak at the R1ex an indicator is required. The root-mean-square value of the random part of the total pressure signal rms is judged to be an adequate indicator as it is not affected by the amount of work done by a particle, nor is the rms signal affected by radial migration effects. The independence of work is important as the work done by the hot gas is higher in comparison to the free stream flow. Regions of high rms are indicative of eddy shedding or regions of high turbulence. The measured level of rms in the hot streak at the stage inlet plane is about twice as high when compared to the free stream. This increased level of rms is convected through the stage and can be tracked at each measurement plane. Using the triple decomposition of the time-resolved pressure signal as shown in Eq. (5) the random part  $p'(t)$  can be evaluated as the difference between the raw pressure  $p(t)$  signal of the high temperature FRAP probe and the phase-locked averaged pressure  $\bar{p} + \tilde{p}(t)$ . The same approach was used by Porreca et al. [23] to derive turbulence quantities:

$$p(t) = \bar{p} + \tilde{p}(t) + p'(t) \quad (5)$$

The data in this experimental study with inlet temperature distortion have been compared to the data presented in the work of Behr et al. [15] using the same turbine configuration without an inlet temperature distortion generator at the same operating conditions. The space time rms diagram in Fig. 10 at 50% span shows where the hot spot is between the rotor wakes. Comparing the rms levels with and without hot spot at midheight, the hot streak is clearly on the pressure side of the rotor wake, indicated by the dashed lines in Fig. 10. Assuming an ideal hot spot with its stagnation pressure at the same level as the free stream, the stator flow field is not affected by the inlet temperature distortion, resulting in constant exit flow angles and Mach numbers. The hot spot travels at higher velocity because it is hotter than the free stream. In the relative rotor blade row frame the hot gas has greater momentum and therefore travels at higher incidence compared to the free stream. This means that the lift distribution on the rotor blade will be strongly affected. As a consequence, and for continuity reasons, the colder fluid has to migrate towards the suction side of the rotor. The tendency for separation of hot and cold gases was first mentioned by Kerrebrock et al. [11] in their work on the effect of the high temperature compressor rotor wakes on downstream stator blades. The same concept is also applicable for turbine blade rows. This tendency for separation of cold and hot gases in the rotor has been experimentally observed by Butler et al. [7]. Three-dimensional unsteady computational investigations by Dorney



(a) 50 Percent Span



(b) 20 Percent Span

**Fig. 10** Space time diagrams of rms signal at R1ex for two different span positions. On the left hand side without hot streak, on the right hand side with hot streak.

et al. [9] and Rai et al. [10] have reported similar findings. Comparing the rms level in the rotor wake at 50% span with and without a hot spot in Fig. 10 shows an augmented rms level for the case with the hot spot. This augmented rms level in the rotor wake either indicates more strongly turbulent boundary layers or stron-

ger trailing edge eddy shedding vorticity originating from the inlet temperature distortion. The hot gases attack the rotor with a higher velocity compared to the free stream, therefore creating a more turbulent boundary layer. The rotor passage vortex at the hub

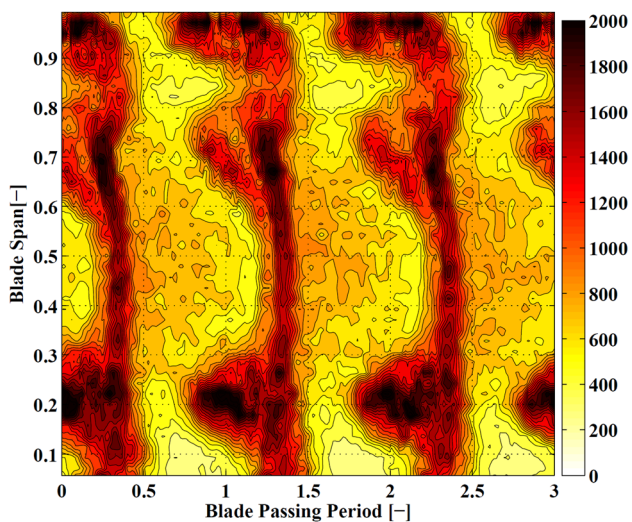


**Fig. 11** Space time diagram of rms signal at R1ex

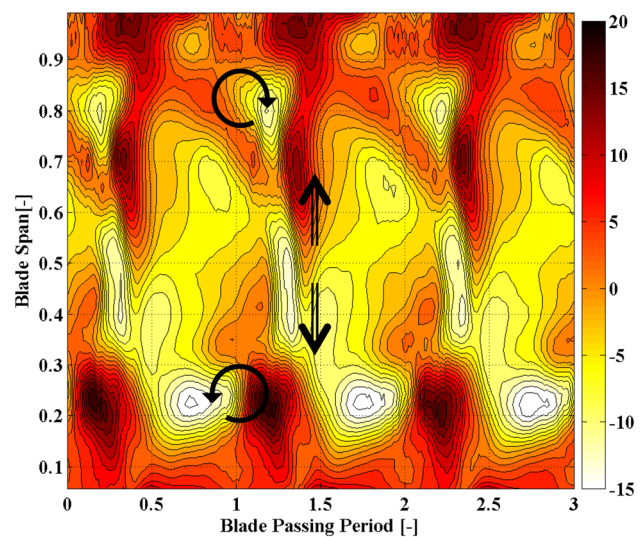


**Fig. 12** Space time diagram of radial velocity  $V_r$  at R1ex

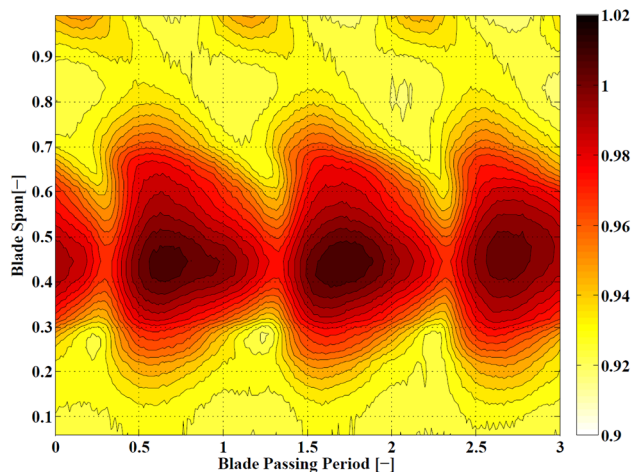


**Fig. 13 Space time diagram of normalized stagnation temperature at R1ex**

(Fig. 10 and 20% span) is modified unsteadily by the hot spot; the rms level gives some idea of where the hot spot fluid is. At the hub the hot gases appear to be on both the pressure and suction sides according to the rms signal, indicating that some of the hot spot is still flowing down the pressure side, while some more has already made its way to the suction side and is caught up in the passage vortex.

Figure 11 shows the rms level for radial traverse through the hot spot as a function of time. As previously mentioned, the high rms zone is clearly on the pressure side, confirming the hot spot to be on the pressure side. Once arriving on the pressure side, the hot gases migrate towards the hub and casing end walls, giving the high rms zone a typical triangular shape. Despite the radial migration the hot spot does not reach the hub and casing end walls for the tested configuration with the hot spot located at 50% span. Figure 12 shows the radial component of the velocity vector at R1ex as a function of time for a traverse going through the hot spot. The radial transport towards the hub and casing can be observed. On the pressure side the two arrows indicate negative  $V_r$  (fluid moving towards the hub) for positions lower than 50% span and positive  $V_r$  (fluid moving towards the casing) for positions higher than 50% span proving radial transport towards hub and casing. The radial migration in particular causes problems at the tip of the blade, a region which is very difficult to cool. Figure 13 confirms these findings based on the FENT probe measurements at R1ex. The hot spot travels slightly radially inwards under the effect of the rotor as the highest measured total temperatures are located at a lower radial position compared to the rotor inlet.

## Conclusions

This paper presents combined time resolved measurements of unsteady pressure, temperature, and entropy in a 1.5-stage unshrouded model axial turbine using the fast aerodynamic response probe (FRAP) and fast entropy probe (FENT) developed at ETH Zurich. The effect of the thermally driven unsteady blade row interactions on the migration and transport mechanisms of hot streaks was measured and analyzed through the whole turbine stage. The hot spot was generated to match nondimensional parameters of real engines at two different peaks to free stream stagnation temperature ratios.

At the exit of the nozzle guide vane the unsteady rotor potential field causes the hot streak to “wobble” in the circumferential direction at rotor blade passing frequency. The highest temperature gases travel about 20% of a pitch under the effect of one rotor blade passing event. The wobbling affects the relative time averaged temperature field at the rotor inlet and thus alters the heat

load on the rotor leading edge by distributing the hot gases over a bigger surface.

Under the influence of the nozzle guide vane the peak of the hot spot migrates about 3% towards the hub casing between the inlet and exit. At the exit of the nozzle guide vane a stronger diffusion towards the suction side of the hot streak was measured (Fig. 7).

Comparing the unsteady temperature measurements at the NGV inlet and outlet showed a reduction of the maximum over free stream temperature ratio by 30%, indicating that enhanced mixing was taking place in the nozzle guide vane. In terms of relative entropy the maximum measured difference between the hot spot and free stream reduces by 30% for the highest temperature gases in the core of the hot spot, indicating a region of heat loss dominating the generated entropy by dissipation and conduction [Eq. (4)]. The maximum drop in circumferentially mass averaged relative entropy in the core of the hot streak is about 21% without the effect of the secondary flow losses for both measurement cases. At the interface of the hot spot with the free stream entropy is generated due to enhanced mixing taking place.

In the rotor relative frame the hot spot is traveling at higher relative total pressure and temperature and therefore at higher incidence and velocity compared to the free stream. It will therefore not be in equilibrium with the rest of the fluid and migrate in the opposite direction to the fluid with lower relative total pressure, toward the pressure side causing an increased heat load on this side of the blade. This migration toward the pressure side has been confirmed by the measurements at the rotor exit with the two different measurement techniques. The measurements also showed that the hot gases migrate radially on the pressure side toward the hub and casing end wall without reaching the end walls (in the measurement configuration radially). The transport of hot gases towards the periphery of the blades causes increased heat loads on the blade tip, a region which is difficult to cool.

## Acknowledgment

The authors thank Michel Mansour from the LEC at ETH Zurich for his help and support during data acquisition with the unsteady entropy probe. The authors would also like to acknowledge the help of Professor Chokani from the LEC in reviewing the paper.

## Nomenclature

$A$	= area ( $\text{m}^2$ )
$h$	= enthalpy ( $\text{J/kg}$ )
$s$	= entropy ( $\text{J/kg}$ )
$\dot{m}$	= massflow ( $\text{kg/s}$ )
$N$	= rotational speed (rps)
$p$	= pressure (Pa)
$\bar{p}$	= time mean part of pressure signal (Pa)
$\tilde{p}$	= periodic part of pressure signal (Pa)
$p'$	= random part of pressure signal (Pa)
$T$	= temperature (K)
$\bar{T}$	= time mean part of temperature signal (K)
$\tilde{T}$	= periodic part of temperature signal (K)
$T'$	= random part of pressure signal (K)
$C_p$	= specific heat capacity ( $\text{J/kg K}^{-1}$ )
$R$	= gas constant ( $\text{J/kg K}^{-1}$ )
$C_{p,r}$	= total pressure coefficient
$Re$	= Reynolds number
$T$	= blade period (s)
$t$	= time (s)
$q$	= amount of heat (J)
$u$	= velocity (m/s)
$v$	= velocity (m/s)
$w$	= velocity (m/s)
$V$	= volume ( $\text{m}^3$ )
$x$	= axial coordinate (m)
$r$	= radial coordinate (m)

## Greek

$\eta$  = efficiency  
 $\theta$  = circumferential coordinate (m)  
 $\mu$  = viscosity (kg/ms)  
 $\Pi$  = pressure ratio  
 $\rho$  = density (kg/m<sup>3</sup>)  
 $\Phi$  = dissipation function (1/s<sup>2</sup>)

## Subscripts

$r$  = radial coordinate  
 $t$  = stagnation flow quantity  
 $s$  = static flow quantity  
 $tt$  = total-to-total  
 $x$  = axial coordinate  
 $\theta$  = circumferential coordinate  
1.5 = total-to-static 1.5 stages

## Abbreviations

FRAP = fast response aerodynamic probe  
FENT = fast entropy probe  
rms = root-mean-square  
NGV1 = first nozzle guide vane  
NGV2 = second nozzle guide vane  
R1<sub>lex</sub> = rotor 1 exit  
R1 = rotor 1  
S1<sub>lex</sub> = stator1 exit  
S1 = stator 1  
S2 = stator 2

## References

- [1] Munk, M., and Prim, R. C., 1947, "On the Multiplicity of Steady Gas Flows Having the Same Streamline Pattern," *Proc. Nat. Acad. Sci. U.S.A.*, **33**(1), pp. 137–141.
- [2] Hermanson, K., and Thole, K. A., 1999, "Effect of Inlet Profiles on Endwall Secondary Flows," *J. Propul. Power*, **16**(2), pp. 286–296.
- [3] Barringer, K. A., Thole, M. P. J. C., and Koch, P. J., 2009, "Migration of Combustor Exit Profiles Through High Pressure Turbine Vanes," *ASME J. Turbomach.*, **131**(2), p. 021010-1–021010-10.
- [4] T. Povey, K. S., Chana, T. J., and Hurrion, J., 2007, "The Effect of Hot Streaks on HP Vane Surface and Endwall Heat Transfer: An Experimental and Numerical Study," *J. Propul. Power*, **129**(1), pp. 32–43.
- [5] Barringer, K., and Polanka, M., 2009, "An Experimental Study of Combustor Exit Profile Shapes on Endwall Heat Transfer in High Pressure Turbine Vanes," *ASME J. Turbomach.*, **131**(2), p. 021009-1–021009-10.
- [6] Jenkins, K. V., and Bogard, D. G., 2004, "The Effects of High Mainstream Turbulence and Turbine Vane Film Cooling on the Dispersion of a Simulated Hot Streak," *ASME J. Turbomach.*, **126**(1), pp. 203–211.
- [7] Butler, T. L., and Sharma, O., 1989, "Redistribution of an Inlet Temperature Distortion in an Axial Flow Turbine Stage," *J. Propul. Power*, **5**(1), pp. 64–71.
- [8] Roback, R., 1993, "Hot streaks and Phantom Cooling in a Turbine Rotor Passage: Part I—Separate Effects," *ASME J. Turbomach.*, **115**(4), pp. 657–666.
- [9] Dorney, R. D., and Edwards, D. E., 1992, "Unsteady Analysis of Hot Streak Migration in a Turbine Stage," *J. Propul. Power*, **8**(2), pp. 520–529.
- [10] Rai, M. M., and Dring, G. P., 1990, "Navier-Stokes Analysis of the Redistribution of Inlet Temperature Distortions in a Turbine," *J. Propul. Power*, **6**(3), pp. 276–282.
- [11] Kerrebrock, J. L., and Mikolajczak, A. A., 1970, "Intra-stator Transport of Rotor Wakes and Its Effect on Compressor Performance," *J. Fluid Mech.*, **92**(1), pp. 359–369.
- [12] Ong, J., and Miller, R., 2008, "Hot Streak Vane Coolant Migration in a Downstream Rotor," Proceedings of ASME Turbo Expo 2008, Vol. 6, pp. 1749–1760.
- [13] Bai-Tao, J. L., and Hong-De, J., 2009, "Combined Unsteady Effects of Hot Streak and Trailing Edge Coolant Ejection in a Turbine Stage," Proceedings of ASME Turbo Expo 2009: Power for Land, Sea and Air.
- [14] Basol, P., Jenny, C. L. A. K., and Abhari, R. S., 2010, "Hot Streak Migration in a Turbine Stage: Effect of Mixing on Hot Streak Attenuation," Proceedings of ASME Turbo Expo 2010.
- [15] Behr, T., Kalfas, A., and Abhari, R. S., 2007, "Unsteady Flow Physics and Performance of a One-and-1/2 Stage Unshrouded High Work Turbine," *ASME J. Turbomach.*, **129**(2), pp. 348–359.
- [16] Kupferschmid, O., Kopperl, W. P. G., and Gyarmathy, G., 2000, "Time Resolved Flow Measurements With Fast Aerodynamic Probes in Turbomachinery," *Meas. Sci. Technol.*, **11**, pp. 1036–1054.
- [17] Lenherr, A. K., and Abhari, R. S., 2010, "High Temperature Fast Response Aerodynamic Probe," Proceedings of ASME Turbo Expo 2010.
- [18] Mansour, N., Chokani, A. K., and Abhari, R. S., 2008, "Unsteady Entropy Measurements in a High Speed Radial Compressor," *ASME J. Eng. Gas Turbines Power*, **130**(2), p. 021603-1–021603-9.
- [19] Mansour, N., Chokani, A. K., and Abhari, R. S., 2008, "Time-Resolved Entropy Measurements Using a Fast Response Entropy Probe," *Meas. Sci. Technol.*, **19**(11), p. 115401.
- [20] Shang, T., and Epstein, A., 1997, "Analysis of Hot Streak Effects on Turbine Rotor Heat Load," *ASME J. Turbomach.*, **119**(1), pp. 544–533.
- [21] Bai-Tao, J. L., and Hong-De, J., 2009, "Numerical Investigation on Unsteady Effects of Hot Streak on Flow and Heat Transfer in a Turbine Stage," *ASME J. Turbomach.*, **131**(3), p. 031015-1–031015-15.
- [22] Rose, M. G., 2009, *Unsteady Flow in Axial Turbines*, Universitaet Stuttgart, Stuttgart, Germany.
- [23] Porreca, M., Hollenstein, A. I. K., and Abhari, R. S., 2007, "Turbulence Measurements and Analysis in a Multistage Axial Turbine," *J. Propul. Power*, **23**(1), pp. 227–234.